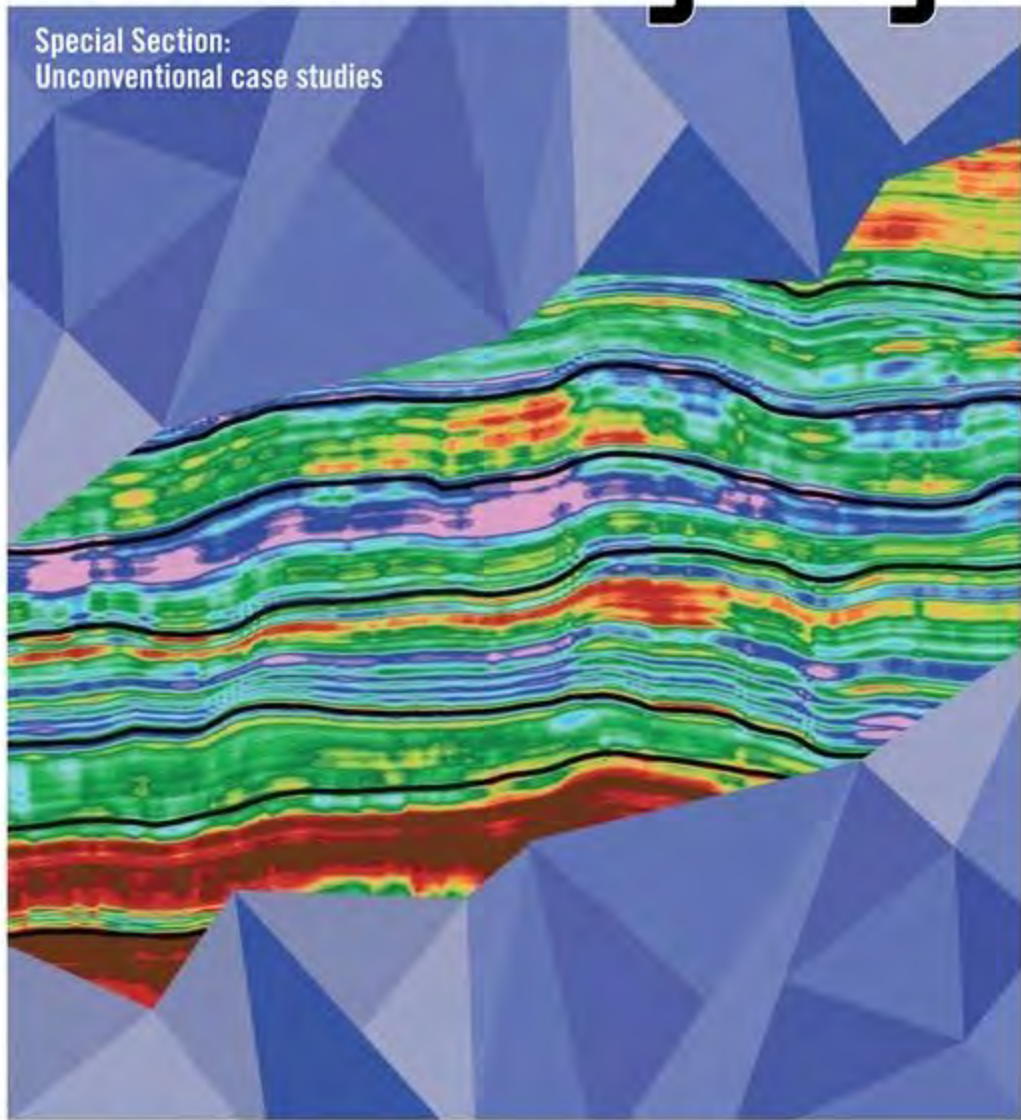


The Leading Edge[®]

Special Section:
Unconventional case studies



SOCIETY OF EXPLORATION
GEOPHYSICISTS

February 2019 - Volume 38, No. 2

ISSN 1070-485X

Calculating far-field anisotropic stress from 3D seismic in the Permian Basin

Michael Shoemaker¹, Santhosh Narasimhan², Shane Quimby³, and James Hawkins¹

<https://doi.org/10.1190/tle38020096.1>

Abstract

Minimum horizontal stress (S_h) is the controlling parameter when hydraulic fracture stimulating tight oil formations but is next to impossible to measure quantitatively, especially in the far field and away from the wellbore. In-situ stress differences between bedding planes control fracture containment, which defines the complexity of fracture propagation and fracture geometry including orientation, height growth, width, and length. Geomechanical rock properties define elastic behavior, influencing how the subsurface will deform under induced stress. These properties include dynamic and static Young's modulus, Poisson's ratio, and Biot's coefficient. When combined with pore pressure and overburden stress, the elastic rock properties describe the mechanical earth model (MEM), which characterizes the geomechanical behavior of the subsurface. The MEM also defines key inputs for calculating S_h using the Ben Eaton stress equation, which has been commonly used by geoscientists for decades. However, calculated S_h from this simple model historically produces uncertain results when compared to field-measured stress due to an assumed homogeneous and isotropic subsurface. This is particularly contrary to tight oil formations that represent shale (or mudrock) reservoirs that are highly laminated and therefore anisotropic. Optimal parameterization of fracture geometry models for well spacing and engineered treatment design requires an anisotropic far-field in-situ stress measurement that accurately captures vertical and lateral variability of geomechanical properties in 3D space. A method is proposed herein that achieves this by using a modified version of the anisotropic Ben Eaton stress model. The method calculates minimum S_h by substitution of inverted 3D seismic volumes directly into the stress equation, replacing the bound Poisson's ratio term with an equivalent anisotropic corrected closure stress scalar (CSS) term. The CSS seismic volume is corrected for anisotropy using static triaxial core and is calibrated to multidomain data types including petrophysics, rock physics, geomechanics, and completion and reservoir engineering field measurements.

Permian Basin field development

Technological advancements in horizontal drilling and hydraulic fracture stimulation of tight oil formations have resulted in the resurgence of the century-old Permian Basin (Figure 1). In fact, the U.S. Energy Information Administration predicts that U.S. crude oil production will average 11.7 million b/d in 2019, which would surpass the previous production record of 9.6 million b/d set in 1970 (EIA, 2018). More than half of this production growth is projected to come from tight oil produced from the Permian Basin. Longer term production growth may be hindered by

“parent-child” or “well-to-well” interference resulting in potentially steeper decline curves from suboptimal fracs. Data suggest the problem may worsen for operators in the Permian as the number of child wells has now reached 50% (Cunningham, 2018) as operators continue to practice more simplified development methods.

Exploration and production companies in the Permian Basin currently implement basin-wide development strategies that involve harvesting-type methods that use multiwell pads to drill stacked horizontal layers. This simple approach uses a repeated sequence implementing identical geometric stage placement and pumping schedules (Shoemaker et al., 2015). Such development strategies fail to recognize subsurface stress heterogeneity and assume similar geomechanical properties that are homogeneous and isotropic. Hydraulic fracture initiation and subsequent geometry are defined by in-situ stress variability, the extent of which defines well economic performance. Assumed isotropic stress states can result in suboptimal hydraulic fracture geometry modeling and treatment design. This can result in well underperformance, particularly as operators continue to develop pads near older (parent) laterals as fields mature. Resultant stress variability from produced fluid depletion or from lithology changes can cause asymmetric fracture geometries, which can alter (child) well performance and ultimate recovery by as much as 25% (Cherian et al., 2018). In addition to parent-child issues, some workers have reported that on average 30% of the perforation clusters in shale rocks are unproductive (Miller et al., 2011), further demonstrating the need for improved development strategies that account for subsurface variability (Warpinski et al., 1987).

In an attempt to mitigate production quandaries in the Permian, current subsurface technology focuses on well spacing with engineered fracture treatment design, which requires hydraulic fracture geometry modeling with accurate subsurface stress inputs. Current methods use an integrated multidomain modeling workflow approach referred to as “seismic to simulation” as presented by Cippola et al. (2011) and Cherian et al. (2018), which is an iterative process centered around fracture geometry modeling. These methods depend on the propagation of geomechanical properties away from available well control, which do not necessarily represent local rock properties at the area of interest (AOI). An amended seismic-to-simulation workflow was adopted for this study that includes the seismic method presented herein (specifically, steps 2 through 6) and follows in ascending order of input:

- 1) Petrophysical modeling: calculate mineralogy compositions, porosity, and saturation models in defining mechanical lithofacies for reservoir and completion quality classification.

¹Callon Petroleum Company, Houston, Texas, USA. E-mail: shoemaker.oilfinder@gmail.com; jhawkins@callon.com.

²Premier Oilfield Group, Houston, Texas, USA. E-mail: santhosh.narasimhan@pofg.com.

³SIGMA Integrated Reservoir Solutions LLC, Houston, Texas, USA. E-mail: stquimby@hotmail.com.

- 2) Seismic interpretation: integrate and tie 3D seismic data to formation tops in time, and convert the seismic horizons/framework to depth for structural and thickness preservation at well control.
- 3) Rock physics modeling: define quantitative elastic seismic response to petrophysics and subsequent mineralogy compositions for reservoir and completion quality integrating lithofacies classification (Dvorkin and Nur, 1996).
- 4) Geologic modeling: construct a 3D geomodel to propagate lithofacies via seismic framework in depth using well control and stochastic algorithms.
- 5) Geomechanics: calibrate geomechanical properties from 3D seismic, logs, and core to diagnostic fracture injection test (DFIT) data using the modified Ben Eaton anisotropic model to estimate near-wellbore and far-field minimum horizontal in-situ stress (Ganpule et al., 2015).
- 6) Fracture modeling: estimate fracture geometry using calculated stress as input to numerical planar fracture simulators, which integrate petrophysics with geomechanics to history match field-measured fracture treatment pressures (Azad et al., 2017) and calibrate to microseismic if available.
- 7) Completion modeling: run sensitivities for optimal well spacing and fracture stimulation parameterization, which includes proppant and fluid type, horizontal cluster spacing, diverters, and stage length.
- 8) Reservoir modeling: perform reservoir simulation and forecasting via iterative history matching of fluid production calibrated to completion modeling (Cherian et al., 2018).

Permian Basin geology

The Midland and Delaware subbasins of the greater Permian Basin (Figure 1) share mutual characteristics such as age and lithology, but depths, nomenclature, and development vary significantly. The focus of this study is the Midland Basin, which likewise demonstrates a high degree of vertical and lateral heterogeneity within the Spraberry and Wolfcamp formations where horizontal wells are landed and fractured within just a few hundred vertical feet of each other and are typically developed via the

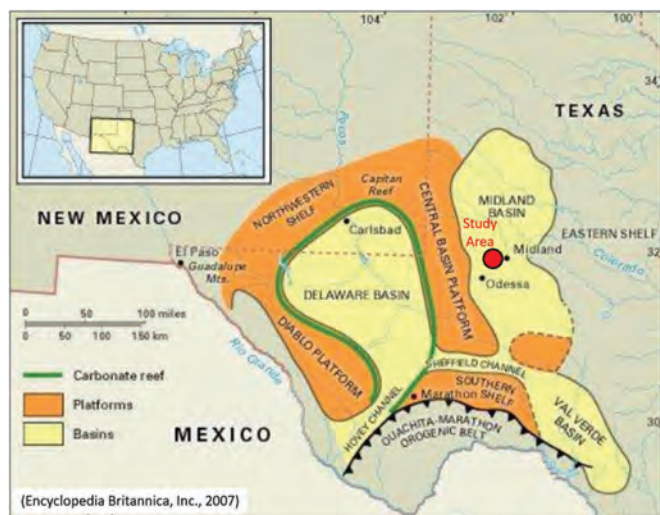


Figure 1. Permian Basin locator with structural features (modified from Encyclopedia Britannica, 2007).

forementioned harvesting approach (Shoemaker et al., 2015). Heterogeneity of rock properties results from the irregular stacking of discrete depositional carbonate units resulting in varying mineralogy compositions (Hobson et al., 1985), which influence elastic geomechanical properties that ultimately define in-situ stress states and fracture complexity. The Spraberry and Wolfcamp formations are highly anisotropic kerogen-rich dark shales and interbedded detrital carbonates, muds, and sands that were deposited predominately by debris/gravity flows and turbidity currents downslope from the Central Basin Platform (CBP) (Figure 1) and likely were deposited in a proximal basin plain environment. Shelfward toward the CBP, carbonate deposition increases with decreasing anisotropy to a point where large detached blocks of dolostone are common proximal to the platform margin. Conceptually, the detrital flows define fairways that have increased carbonate mineralogy compositions with proportionally less clay and therefore are mechanically less ductile and represent locations that are potentially less anisotropic and more conducive to hydraulic fracture stimulation. These mineralogical changes in lithofacies drive fracture geometry and completion optimization and represent areas of in-situ stress variability that the seismic method, presented herein, attempts to measure away from well control.

Elastic surface seismic response to lithofacies was quantified using the petrophysics model integrated with a rock physics template (RPT) shown in Figure 2. The petrophysics model,

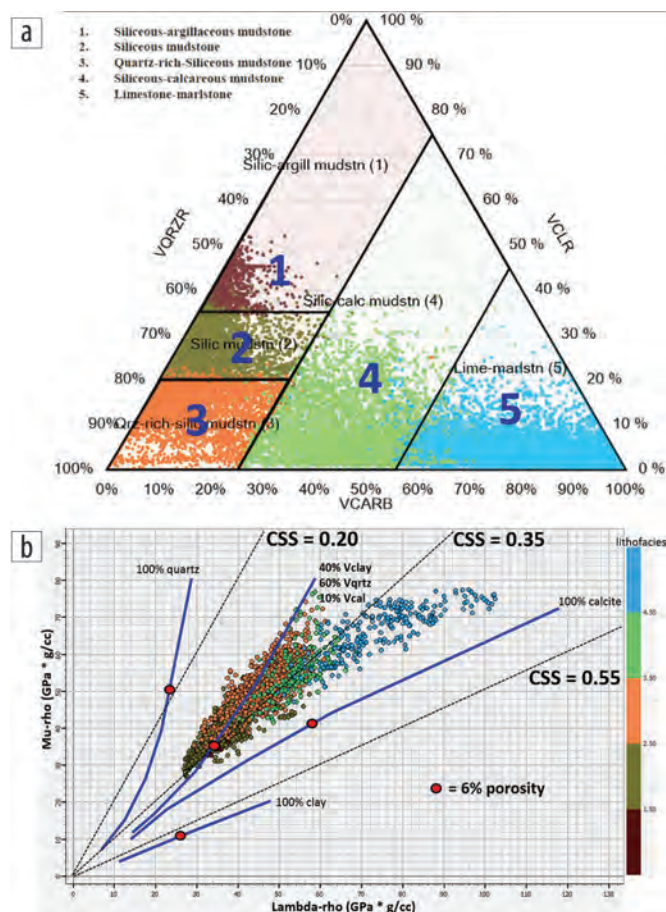


Figure 2. (a) Ternary diagram showing lithofacies classification from petrophysics modeling and (b) RPT integrated with the lithofacies.

represented by a ternary mineralogical distribution plot, was generated using static core and dynamic triple combo data. Spraberry and Wolfcamp formations were combined and grouped into five separate geomechanical lithofacies based on clustering of stratigraphic and mineralogical changes and listed in ascending order of increasing “brittleness.” Quantified elastic seismic response to geomechanical properties, and thus in-situ stress states, can also be analyzed combining said lithofacies with RPTs (Vernik, 2016). A lambda-rho versus mu-rho RPT (Figure 2) was created using Hashin-Strikman-based bounds (Dvorkin and Nur, 1996) with mineralogical elastic constants defined by Sayers et al. (2015).

In-situ stress and geomechanics

In-situ stress state is the most important factor that controls hydraulic fracture stimulation and complexity (Warpinski et al., 1987; Iverson, 1995) but is next to impossible to measure quantitatively, especially in the far field and away from the wellbore in 3D space. Minimum horizontal stress (S_h) is one of three principle stresses that describe the subsurface stress state, and its magnitude controls the propagation of hydraulic fracture stimulation (Ma and Holditch, 2016), which ultimately determines the success of a well and its economic performance. When induced injection pressures exceed S_h , fractures generally occur and will propagate orthogonally toward the direction of S_h within a path of least resistance determined by stratigraphic (or geomechanical) contrasts. In-situ stress differences between bedding planes control fracture containment vertically and laterally, which defines the complexity of fracture propagation and fracture geometry characteristics such as height growth, length, and width that ultimately control proppant placement, drainage, and well spacing (Ganpule et al., 2015). Geomechanical rock properties from mineralogical compositions define elastic behavior and tensile strength, influencing how the subsurface will deform under induced stress and strain, which are governed by elastic rock properties such as Young’s modulus, Poisson’s ratio, and Biot’s coefficient.

The mechanical earth model

When combined with pore pressure and overburden stress, the elastic properties describe the mechanical earth model (MEM), which characterizes the geomechanical behavior of the subsurface. The MEM (Figure 3) acts as both a diagnostic and predictive tool defining key inputs for calculating minimum S_h using an isotropic uniaxial strain-based model defined in terms of the Ben Eaton stress equation, which has been commonly used by geoscientists for decades to calculate subsurface stress. However, calculated S_h from this simple model historically produces uncertain results (Barree et al., 2009) when compared to field-measured stress (Iverson, 1995) due to an assumed homogeneous and isotropic subsurface. This is particularly contrary to tight oil formations,

which represent shale (or mudrock) reservoirs that are highly variable and laminated and are anisotropic representing vertical transverse isotropic (VTI) media (Sayers, 2010). Likewise, more complex models require rock parameterization based on laboratory (static core) measurements (Thiercelin and Plumb, 1994; Singleton, 2018a), but quantitative geomechanical measurements are rare to obtain. This reflects a current inability to accurately predict far-field in-situ stress (Iverson, 1995) for fracture geometry estimation and effective hydraulic fracture treatment design that accounts for far-field virgin subsurface variability.

Closure stress scalar

The closure stress scalar (CSS) represents a unique elastic rock property also characterized by the MEM (Figure 3) but defined as a function of Lamé elastic constants (Goodway, 2010; Close et al., 2012) where lambda (λ) is incompressibility and mu (μ) is shear modulus. The calculated CSS results in improved vertical and lateral geomechanical variability (Goodway et al., 1997; Goodway et al., 2010) along horizontal wellbores and far field and is ultimately corrected for anisotropy using static triaxial core (Higgins et al., 2008). The CSS is equivalent to the bound Poisson’s ratio term ($\frac{\nu}{1-\nu}$) embedded in the isotropic Ben Eaton model (or uniaxial stress equation) historically used to calculate minimum S_h :

$$S_h = \frac{\nu}{1-\nu} (S_v - \alpha P_p) + \alpha P_p, \quad (1)$$

where S_h equals the induced stress required to fracture the rock given ν or Poisson’s ratio, the overburden stress (S_v), Biot’s coefficient (α), and pore pressure of the formation (P_p). For CSS, lambda (λ) and mu (μ) define Hooke’s law relating stress to strain (Sayers, 2010), which intrinsically defines the fracability of brittle (low-stress) rocks and ductile (higher stress) rocks. Likewise, Goodway et al., (2010) and Close et al. (2012) define the CSS in terms of λ and μ , which is equivalent to the bound Poisson’s ratio term defined in equation 1 or:

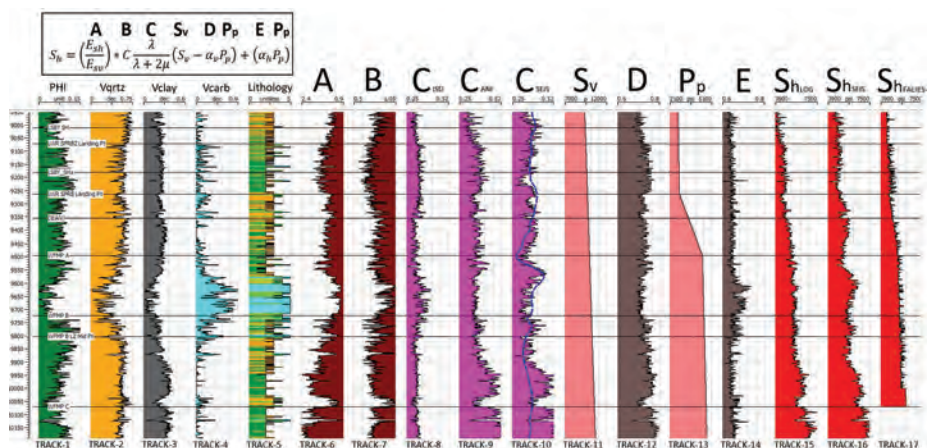


Figure 3. 1D MEM used for this study with the uniaxial strain equation for minimum S_h . Equation terms are labeled. Location is defined in Figure 5 (maps E and F) at pad C. The upper lower and lower Spraberry landing zones are labeled just above the Dean Formation.

$$CSS_{ISO} = \frac{\lambda}{\lambda + 2\mu} = \frac{\nu}{(1-\nu)}, \quad (2)$$

where CSS represents an isotropic rock quality term calculated quantitatively from the amplitude variation with offset (AVO) seismic inversion discussed later.

Method

A process is proposed herein that has successfully measured far-field in-situ stress states using a modified version of the anisotropic Ben Eaton stress model presented by Narasimhan et al. (2016) and amended to the seismic-to-simulation workflow defined by Cippola et al. (2011) and Cherian et al. (2018). The new model calculates minimum S_h by substitution of prestack simultaneous inverted 3D seismic volumes (Gray, 2002; Singleton, 2018b) directly into the uniaxial stress equation by replacing the bound Poisson's ratio term with an equivalent CSS term extracted from surface seismic data.

A model-based simulated annealing numerical method was implemented for the elastic (AVO) seismic inversion, which was ultimately used to calculate the CSS. An Aki and Richards (1980) linearized approach to approximate Zoeppritz (1919) equations was used to generate elastic geomechanical properties including broadband compressional-wave velocity (V_p) and shear-wave velocity (V_s), which were used to calculate Poisson's ratio from the seismic. Prestack common midpoint gathers were conditioned to enhance signal to noise. For added sensitivity to vertical and horizontal in-situ stress variability, inverted elastic parameters were recast into equivalent terms of Lamé elastic constants (Goodway et al., 1997; Goodway et al., 2010; Close et al., 2012) defined by lambda (λ) or incompressibility and mu (μ) for shear rigidity and were used to calculate the CSS.

CSS volumes derived from AVO seismic inversion were calibrated and quantitatively interpreted using the RPT defined in Figure 2. Constant lines of CSS, calculated from dynamic log data, were used to characterize the geomechanical seismic response to mineralogy compositions. For example, lithofacies-2 and particularly lithofacies-3 are characteristic of greater volume of quartz and carbonate and have potentially lower stress (or CSS magnitude) and require less induced stress to fracture the rock. Incidentally, these would represent ideal isotropic areas to land wells for optimal fracture initiation and fracture geometry. Greater volumes of carbonate representing lithofacies-4 and 5 can conversely act as fracture barriers or baffles by limiting fracture height growth vertically and laterally.

Anisotropic correction scalar

For VTI media representing anisotropic shale, Thomsen (2013) and Sayers et al. (2015) both argue that the industry needs to integrate anisotropy effects into seismic methods that are currently being implemented to extract geomechanical and stress properties from shale. Local anisotropy effects used herein were investigated and measured using dynamic compressional sonic and shear logs calibrated to static triaxial core data (Barree et al., 2009) from the area. Narasimhan et al. (2016) provide a valid workflow, implementing a Ben Eaton anisotropic stress model

for converting static mechanical measurements from core to dynamic velocity measurements using empirical models calibrated to the area. Resulting anisotropic scalars, representing correction factors to isotropic terms defined in equation 2, are defined in equation 3:

$$S_b = \left(\frac{E_{sh}}{E_{sv}} \right) \frac{\nu_{sv}}{1-\nu_{sh}} (S_v - \alpha_v P_p) + (\alpha_b P_p), \quad (3)$$

where $\frac{E_{sh}}{E_{sv}}$ is Young's modulus (or anisotropic modulus) from triaxial core measured in the horizontal and vertical directions, and $\frac{\nu_{sv}}{(1-\nu_{sh})}$ is the anisotropic bound Poisson's ratio from triaxial core measured in the horizontal and vertical directions, as is α_h and α_v , respectively, which define the anisotropic Biot's coefficient. This data in log form represent anisotropic components of the MEM shown in Figure 3.

The difference in magnitude between the isotropic and anisotropic bound Poisson's ratio can then be calculated to represent an anisotropic correction scalar (ACS) magnitude that's applied to the isotropic CSS defined in equation 2, which now becomes:

$$CSS_{ANI} = C \frac{\lambda}{\lambda + 2\mu} = \frac{\nu_{sv}}{(1-\nu_{sh})}, \quad (4)$$

where C is the ACS, which equals the isotropic bound Poisson's ratio less any anisotropic effects (when $C=1$). Equation 4 defines the CSS corrected for VTI media and can now be inserted into equation 3 and minimum S_h solved for using CSS extracted from the AVO inverted seismic where:

$$S_b = \left(\frac{E_{sh}}{E_{sv}} \right) * C \frac{\lambda}{\lambda + 2\mu} (S_v - \alpha_v P_p) + (\alpha_b P_p). \quad (5)$$

Results: Example from the Midland Basin

Figure 3 defines the MEM representing this study and AOI and relates mineralogy and lithofacies to geomechanics and rock physics defined in Figure 2. The MEM defines overburden stress and pore pressure gradients calibrated to DFIT and dynamic log measurements (Narasimhan et al., 2016; Cherian et al., 2018) and assumes VTI media representing anisotropic shale (Sayers, 2010). All terms defined in equation 5 are shown in log form and are equally depth sampled at 1 ft including the CSS volume derived from AVO seismic inversion.

Excluding the seismic-defined CSS, all terms from equation 5 that define the MEM in Figure 3 were simply interpolated away from the MEM location to areas of interest using the depth-converted seismic framework and existing vertical wells (not shown) as modeling constraints to preserve geologic structure and formation thickness. The end result is seven 3D rock property cubes (Figure 4) representing each of the terms defined in equation 5 with each

cube sampled equally at 1 ft, including the seismic-defined CSS term.

Stress maps (Figure 5) extracted from the final minimum S_h volume outline the AOI located in the Midland Basin (Figure 1), which has been subdivided into areas representing three horizontal well pads (A, B, and C). They were landed in the upper lower Spraberry (map E) and the lower Spraberry (map F), which are vertically separated by approximately 200 ft. Pads A and B were each developed similarly using a six-well chevron-type pattern (Shoemaker et al., 2015) with three laterals landed in the upper lower Spraberry (odd numbered wells) and three wells in the lower Spraberry (even numbered wells). Both six-well pads were zipper fractured with duel fracture crews to minimize stress shadowing for enhanced production. Pad C was landed in the lower Spraberry only and represents a four-well pad drilled significantly earlier than the other pads.

An example regional cross section in depth (Figure 5) with horizons is displayed from north to south (or from pads A to C), which shows minimum S_h calculated from core and logs only compared to the final S_h solution (panel D) that integrates the rich geo-mechanical variability from the CSS seismic. Notice along the cross sections the two Spraberry landing zones just above the Dean Formation, which are identified by lateral wells (by pad) for reference. The upper Spraberry landing zone in this part of the basin (wells A5 and B5 from pads A and B) is typically characteristic of a higher volume of clay (yellow) and is thus more ductile, representing lithofacies-2 (Figure 2). This increases the induced stress required to fracture the rock by as much as 1200 psi, greatly influencing fracture geometry and subsequent treatment design for optimal well performance.

Quantitatively, the higher stress effect in the upper zone decreases at northern (blue) areas of the AOI at pad A (Figure 5, map E) where lower CSS magnitude reflects a greater proportion of carbonate rock versus clay, which is confirmed by vertical wells in the area. Likewise, the lower Spraberry landing also shows relatively more brittle rock (map F). Consequently, both zones in this part of the basin at pad A represent lithofacies-3, which suggests a less aggressive fracture treatment design with perhaps greater stage and cluster spacing. At pad B, stress maps differ, confirming

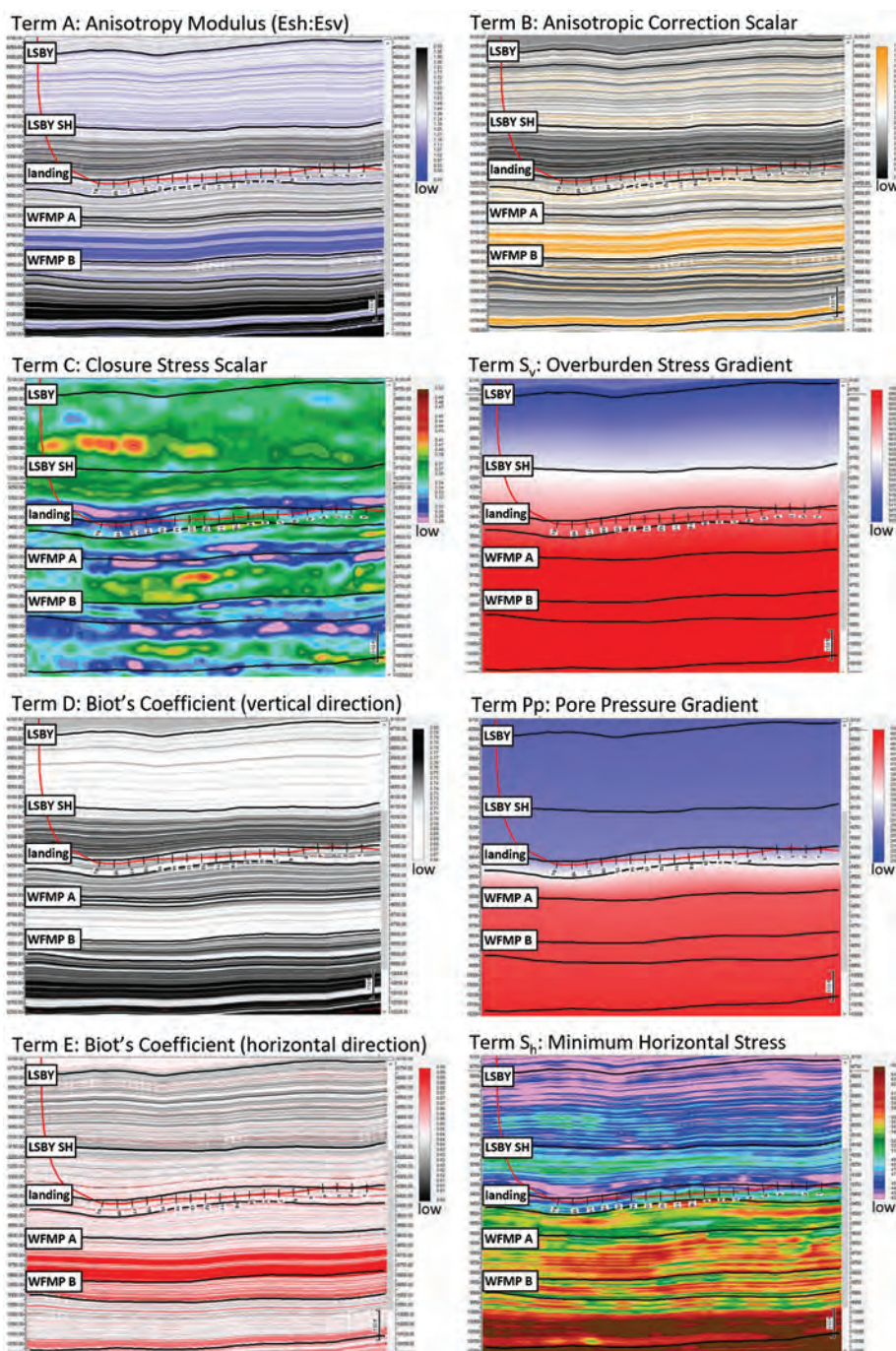


Figure 4. Cross section examples from the 3D cubes representing each of the seven uniaxial stress equation terms defined by the MEM in Figure 3. Cross sections were extracted along horizontal well C1 (pad C). The lower Spraberry landing zone is labeled. The final minimum S_h solution is represented by the lower right cross section (S_h). Notice the added stress variability provided by the seismic.

a much greater in-situ stress for the upper landing zone (map E, red) and relatively less stress for the lower landing (map F, purple). The relatively higher far-field stress characteristic of the upper landing may be conducive to increased fracture containment, representing potential areas that may be less prone to parent-child depletion issues or areas with less probable well-to-well fracture bashing contrary to (purple) low-stress areas that are potentially more prone to asymmetric fracture geometries and well-to-well “frac hits.” Far-field and near-wellbore fracture geometry can now

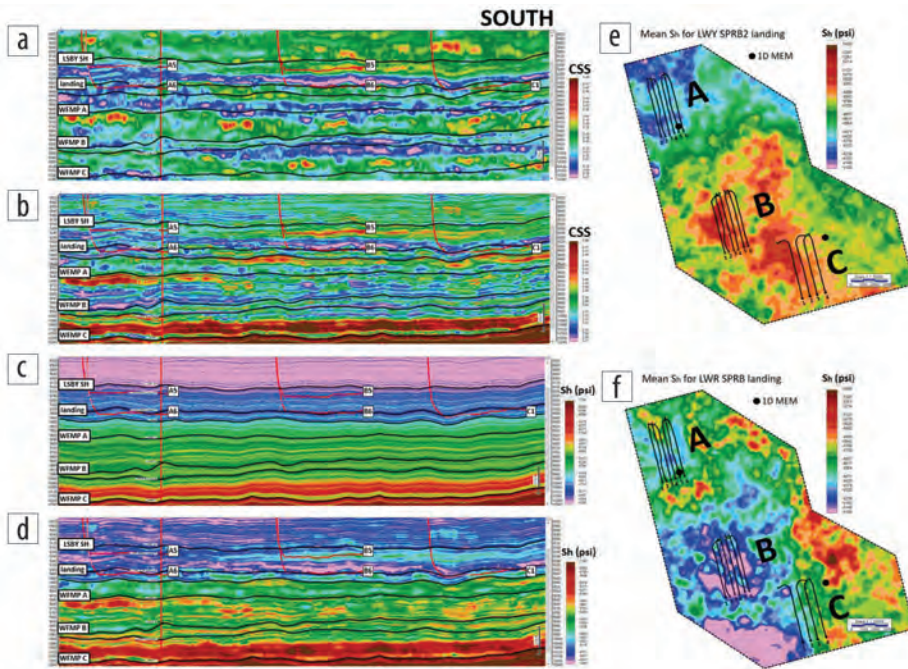


Figure 5. A regional cross section is shown with horizontal wellbores traversing from north to south (from well pads A, B, and C). For all cross sections and maps presented herein, hot red/yellow colors define areas of greater in-situ stress (more ductile), and cooler blue/purple colors define relatively less stress (more brittle). Pads A and B were each developed using a six-well chevron-type pattern with three laterals landed in the upper lower Spraberry (odd numbered wells) and three wells in the lower Spraberry (even numbered wells). The MEM (Figure 3) location near pad C is shown. Panel A shows CSS from AVO seismic inversion only compared to an identical cross section with ACSs from triaxial core applied (panel B). Panel C shows anisotropic minimum S_h calculated from core and logs only compared to panel D, which shows an identical cross section at log resolution but with CSS from the AVO seismic. Notice the added geomechanical variability the seismic provides. Also shown are regional (S_h) maps representing the upper lower Spraberry landing zone (panel E) and the lower Spraberry landing zone (panel F).

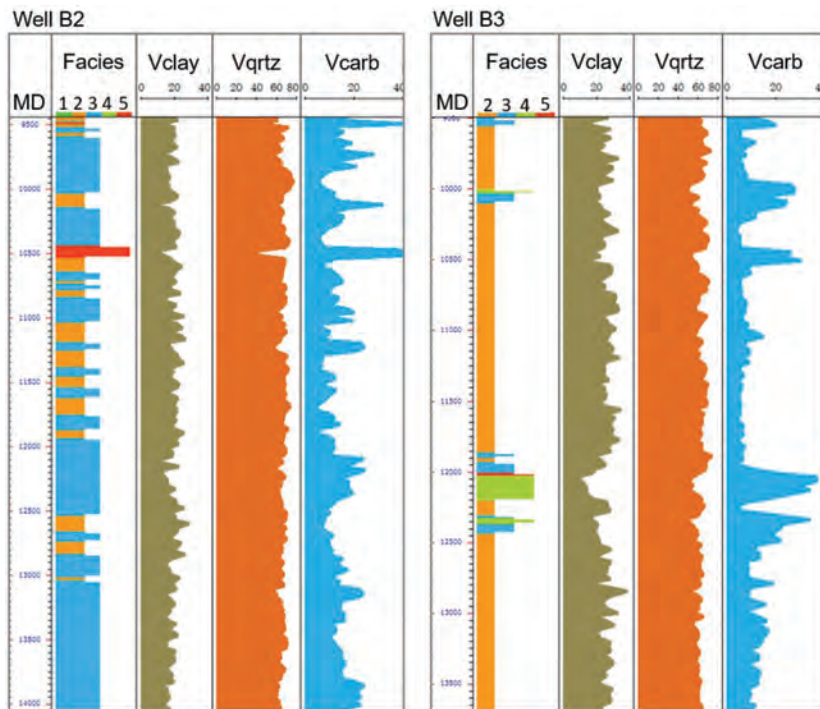


Figure 6. XRD and XRF geochemical analysis of cuttings show mineralogy compositions by volume for horizontal wells B2 (lower Spraberry landing) and B3 (upper lower Spraberry landing) located at well pad B (Figure 5). Well B2 is characteristic of lithofacies-3 (Figure 2) compared to well B3, which on average shows 30% more clay and is represented by lithofacies-2 with subsequent higher stress and ductility requiring a more aggressive fracture treatment.

be modeled for optimal well spacing and engineered treatment design including stage and cluster spacing along the horizontal wellbores.

The significant vertical stress contrasts, related to the Spraberry landing zones, have also been confirmed by drill cuttings implementing x-ray diffraction (XRD) and x-ray fluorescence (XRF) geochemical analysis for mineralogy compositions along horizontal wells B2 and B3 (at pad B) where cuttings were acquired. Figure 6 summarizes these results and shows that the upper lower Spraberry zone (well B3) contains by volume up to 30% more clay than the lower Spraberry landing zone. Additional validation from other independent measurements can come from horizontal MWD logs and drilling data with an example shown in Figure 7 from well A6 (pad A) from the lower Spraberry landing zone. While drilling, greater rate of penetration (ROP) values generally correspond to higher clay volumes encountered along the lateral, which incidentally is confirmed by greater gamma ray measurements and volume of clay from cuttings where higher in-situ stress states exist from the geomechanics. Development strategies involving acreage prioritization can now be optimized regionally and governed by in-situ stress variability.

At present, other seismic methods assume isotropy and do not necessarily account for anisotropy stress in shale formations (Thomsen, 2013; Sayers et al., 2015), which can result in significant errors when estimating geomechanical properties and stress from seismic. For example, Figure 8 shows cross sections along well C4 (pad C) landed in the lower Spraberry. Notice that the isotropic CSS, calculated from both seismic and logs (top panels), underestimates low closure stress values at Wolfcamp flooding surfaces (i.e., WFMP A, WFMP B, and WFMP C) representing organic-clay-rich source rocks (lithofacies-1) that are significantly anisotropic. Increased stress values (from static triaxial core) result after anisotropy scalar corrections are applied to the isotropic values.

Direct application of the method is further summarized in Figures 9 and 10,

Figure 7. (a) Minimum S_h cross section lengthwise along horizontal well A6 (pad A) and (b) independent measurements comparing S_h extracted horizontally along the wellbore in MD compared to: ROP, MWD gamma ray, and volume of clay from XRD and XRF geochemical analysis. Drill bit ROP typically increases within relatively larger volumes of clay horizontally representing higher stress and gamma ray measurements, which are shown.

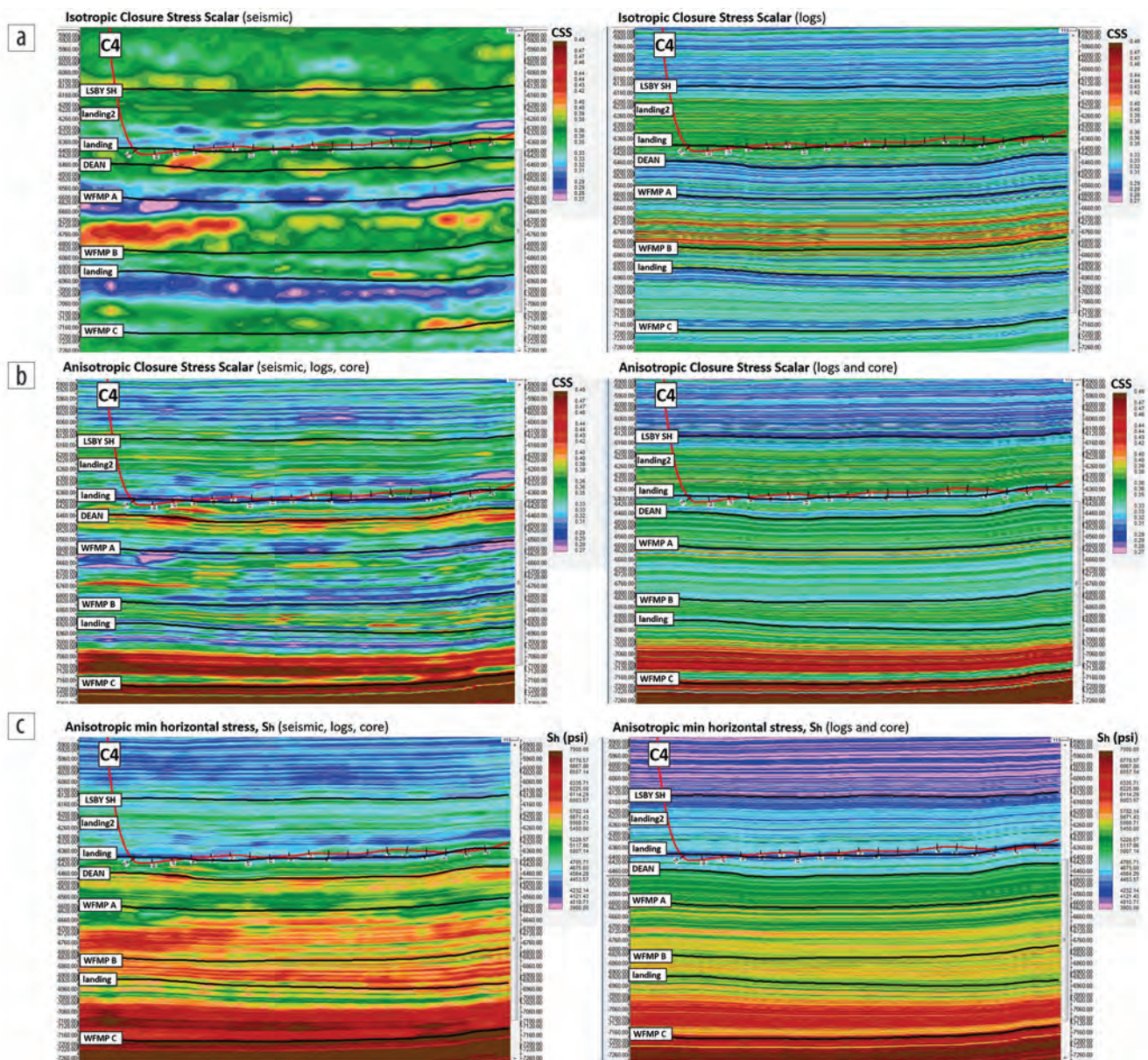
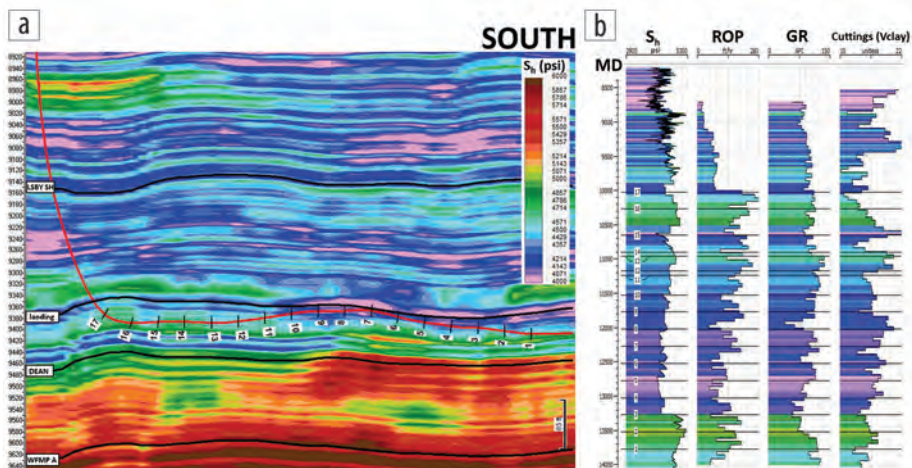


Figure 8. An arbitrary cross section extracted along horizontal well C4 at pad C. The top-left panel A shows the isotropic CSS from AVO seismic inversion compared to CSS calculated from dynamic logs only (right, panel A). Middle-left panel B shows CSS from AVO seismic corrected for anisotropy effects using scalar terms A and B (equation 5) compared to the same cross section but with CSS calculated from logs only (middle-right panel B). The bottom-left panel C compares minimum S_h calculated with CSS from AVO seismic inversion compared to S_h calculated from CSS using logs only (right). Notice the added geomechanical and stress variability provided by the seismic (left panels). Both lower Spraberry landing zones are shown as well as the Wolfcamp B landing.

which focus on the six wells representing pad B (Figure 5, maps E and F). A minimum S_h cross section in depth (Figure 9) was extrapolated from the S_h volume lengthwise along wellbores B5 and B6 representing the upper lower Spraberry and lower Spraberry landing zones, respectively. Vertical and lateral in-situ stress can vary by as much as 2000 psi vertically from the wellbores and far field, which is confirmed by the stress maps representing the landing zones.

This is particularly apparent from the cross section at the Dean surface, which can act as a fracture barrier to downward propagating hydraulic fractures initiated from the lower landing zone. As mentioned earlier, the significant in-situ stress contrast between the upper and lower landing zones is also apparent in the cross section, which can vary by as much as 1200 psi. This vertical difference in stress results from the change in elastic properties from the addition of clay, which can constrain fracture propagation from the lower zone, preventing production thieving from the upper zone. The stress volume can aid in determining vertical well spacing and treatment design ahead of the drill bit.

Lateral contrasting stress states can also affect fracture propagation and geometry. Stress maps (Figure 9) representing the landing zones show significant lateral stress variability potentially affecting the complexity of fracture initiation, length, and height. The maps show the potential for fracture asymmetry particularly within (purple) areas of low stress toward the toe of the lower Spraberry wells (B2, B4, and B6). For example, less aggressive fracture stimulation at these areas is perhaps warranted to minimize asymmetry effects.

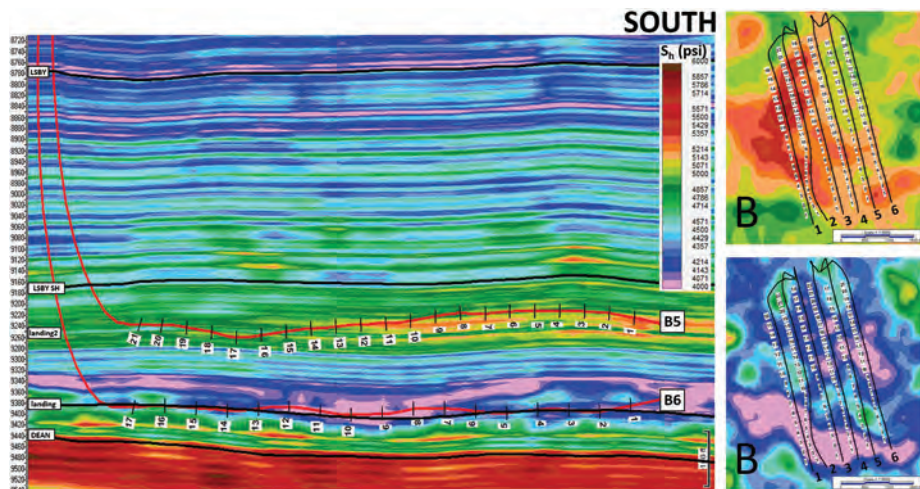


Figure 9. A cross section representing minimum S_h at 1 ft vertical log resolution along the B5 and B6 horizontal wellbores (pad B, Figure 5) representing the upper lower Spraberry and lower Spraberry landing zones, respectively. Maps show the S_h variability between the two landing zones, reflecting the significant stress contrast seen in the cross section. For all cross sections and maps, hot red/yellow colors define areas of greater in-situ stress (more ductile) and cooler blue/purple colors define relatively less stress (more brittle).

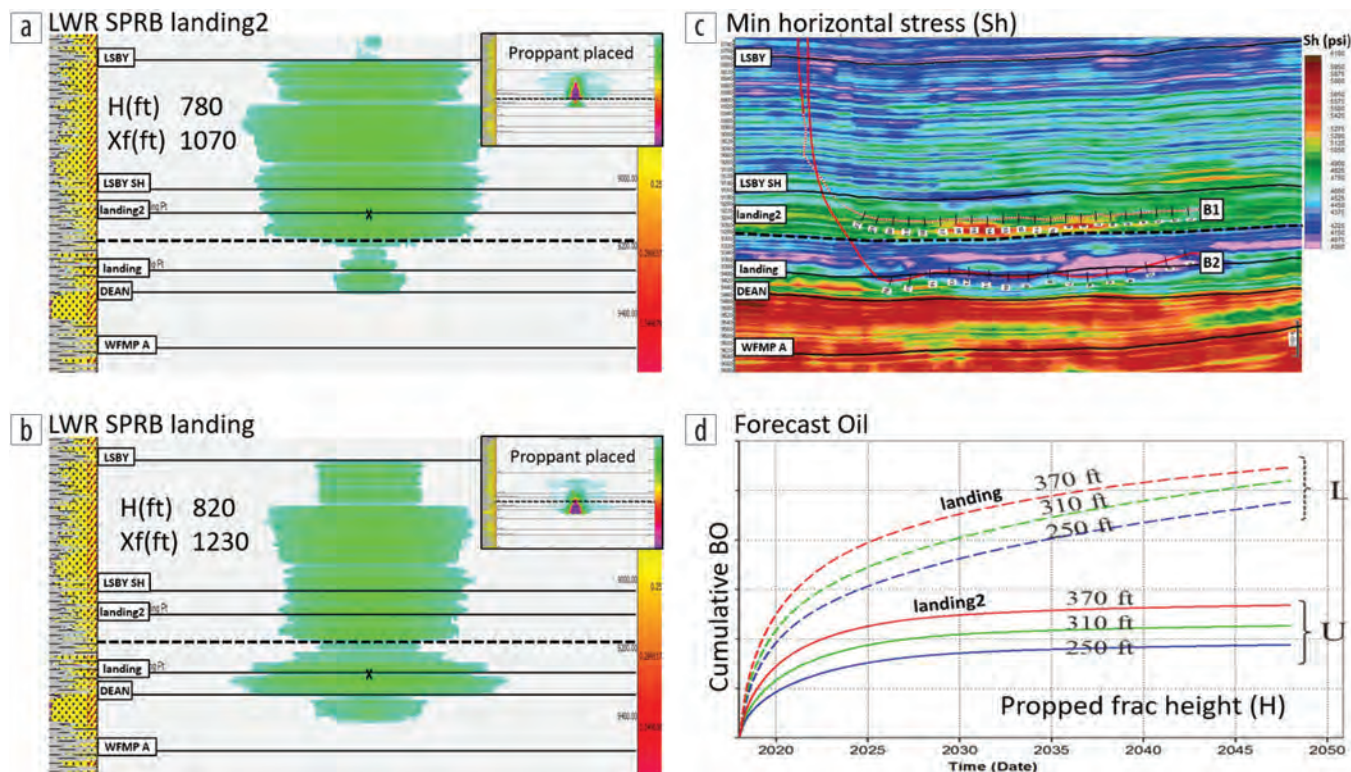


Figure 10. Fracture geometry models run using identical hydraulic fracture treatment designs representing (a) the upper lower Spraberry landing zone and (b) the lower Spraberry landing zone representing (c) wells B1 and B2. Vertical depth exaggeration of fracture models and cross section are the same for identical comparison. (d) Modeled hydrocarbon production of the two landing zones using identical treatment designs. The top profile highlights more production from the lower Spraberry landing zone characteristic of ideal geomechanics (lithofacies-3) and brittleness (less clay and stress) relative to the upper landing zone representing lithofacies-2, which contains more clay for added ductility and stress and thus requires a more aggressive fracture design with tighter stage and cluster spacing to enhance production.

Figure 10 shows fracture geometry models that were run using identical treatment designs and were initiated in each of the lower Spraberry landing zones. The lower zone models a fracture geometry with a higher fracture height and length relative to the upper lower zone, which shows a less-efficient fracture. As mentioned, the upper zone contains upward of 30% more clay (lithofacies-2) thus requiring a more aggressive fracture with tighter stage and cluster spacing. This is further substantiated from the hydrocarbon production model (Figure 10d), which was completed using identical treatment designs for both zones and further demonstrates a more optimal fracture with enhanced production from the lower zone due to improved geomechanics that support a less aggressive treatment design relative to the upper landing zone.

Conclusions

The minimum S_h volume presented herein has been corrected for anisotropy using triaxial core and can be directly input into fracture geometry simulators with the necessary far-field and virgin geomechanical variability provided by 3D seismic. Most current methods used to infer stress are nonunique and require calibration to existing data and measure, for example, indirect data representing pressure “hits” from offsetting wells or methods representing workflows that require propagation of geomechanical properties away from well control. Said methods infer measurements that do not necessarily represent rock properties at the AOI, particularly in 3D space.

The method presented herein successfully integrates multi-domain data sets with AVO seismic inversion expressed in terms of Lamé elastic parameters for added horizontal and vertical elastic variability and effectively measures far-field stress for fracture geometry modeling and fracture treatment optimization away from the wellbore. The stress volume can be interpreted qualitatively for wellbore stability applications and can provide stress measurements quantitatively for optimal field development strategies including vertical and lateral well spacing. It can be used as a mitigation tool ahead of the drill bit in areas affected by parent-child and well-bashing issues. **IME**

Data and materials availability

Data associated with this research are confidential and cannot be released.

Corresponding author: shoemaker.oilfinder@gmail.com

References

Aki, K., and P. G. Richards, 1980, *Quantitative seismology: Theory and methods*: W. H. Freeman and Co.

Azad, A., K. Somanchi, J. R. Brewer, and D. Yang, 2017, Accelerating completions concept select in unconventional plays using diagnostics and frac modeling: Presented at Hydraulic Fracturing Technology Conference and Exhibition, SPE, <https://doi.org/10.2118/184867-MS>.

Barree, R. D., J. V. Gilbert, and M. Conway, 2009, Stress and rock property profiling for unconventional reservoir stimulation: Presented at Hydraulic Fracturing Technology Conference and Exhibition, SPE, <https://doi.org/10.2118/118703-MS>.

Cherian, B., M. Shoemaker, S. Nwoko, S. Narasimhan, O. Olaoye, J. Iqbal, and N. Zakhour, 2018, Understanding development

drivers in horizontal wellbores in the Midland Basin: Presented at Liquids-Rich Basins Conference, SPE, <https://doi.org/10.2118/191782-MS>.

Cipolla, C. L., T. Fitzpatrick, M. J. Williams, and U. K. Ganguly, 2011, Seismic-to-simulation for unconventional reservoir development: Presented at Reservoir Characterization and Simulation Conference, SPE, <https://doi.org/10.2118/146876-MS>.

Close, D., M. Parez, B. Goodway, and P. Purdue, 2012, Integrated workflows for shale gas and case study results for the Horn River Basin, British Columbia, Canada: *The Leading Edge*, **31**, no. 5, 556–569, <https://doi.org/10.1190/tle31050556.1>.

Cunningham, N., 2018, Why U.S. shale may fall short of expectations, <https://oilprice.com/energy/crude-oil/why-US-shale-may-fall-short-of-expectations.html>, accessed 11 November 2018.

Dvorkin, J., and A. Nur, 1996, Elasticity of high-porosity sandstones: Theory for two North Sea data sets: *Geophysics*, **61**, no. 5, 1363–1370, <https://doi.org/10.1190/1.1444059>.

EIA, 2018, Permian region is expected to drive U.S. crude oil production growth through 2019, <https://www.eia.gov/todayinenergy/detail.php?id=36936>, accessed 7 January 2019.

Ganpule, S. V., K. Srinivasan, T. Izykowski, B. A. Luneau, and E. Gomez, 2015, Impact of geomechanics on well completion and asset development in the Bakken Formation: Presented at Hydraulic Fracturing Technology Conference and Exhibition, SPE, <https://doi.org/10.2118/173329-MS>.

Goodway, B., 2010, The magic of Lamé: *The Leading Edge*, **29**, no. 11, 1432–1432, <https://doi.org/10.1190/tle29111432.1>.

Goodway, B., M. Perez, J. Varsek, and C. Abaco, 2010, Seismic petrophysics and isotropic-anisotropic AVO methods for unconventional gas exploration: *The Leading Edge*, **29**, no. 12, 1500–1508, <https://doi.org/10.1190/1.3525367>.

Goodway, B., T. Chen, and J. Downton, 1997, Improved AVO fluid detection and lithology discrimination using Lamé petrophysical parameters; “ $\lambda\rho$ ”, “ $\mu\rho$ ”, & “ λ/μ fluid stack”, from P and S inversions: 67th Annual International Meeting, SEG, Expanded Abstracts, 183–186, <https://doi.org/10.1190/1.1885795>.

Gray, D., 2002, Elastic inversion for Lamé parameters: 72nd Annual International Meeting, SEG, Expanded Abstracts, 213–216, <https://doi.org/10.1190/SEGAB.21>.

Higgins, S. M., S. A. Goodwin, A. Donald, T. R. Bratton, and G. W. Tracy, 2008, Anisotropic stress models improve completion design in the Baxter Shale: Presented at Annual Technical Conference and Exhibition, SPE, <https://doi.org/10.2118/115736-MS>.

Hobson, J. P., C. D. Caldwell, and D. F. Toomey, 1985, Early Permian deep-water allochthonous limestone facies and reservoir, West Texas: *AAPG Bulletin*, **69**, no. 12, 2130–2147.

Iverson, W. P., 1995, Closure stress calculations in anisotropic formations: Presented at Low Permeability Symposium, SPE, <https://doi.org/10.2118/29598-MS>.

Ma, Y., and S. Holditch, 2016, *Unconventional oil and gas resources handbook*: Elsevier.

Miller, C. K., G. A. Waters, and E. I. Rylander, 2011, Evaluation of production log data from horizontal wells drilled in organic shales: Presented at North American Unconventional Gas Conference and Exhibition, SPE, <https://doi.org/10.2118/144326-MS>.

Narasimhan, S., H. Shaikh, J. K. Gray, B. V. Cherian, O. Olaoye, R. Rifai, and M. Sharf-Aldin, 2016, Effect of horizontal stress models and Biot poro-elasticity on predicted fracture geometry: SPE, <https://doi.org/10.2118/179162-MS>.

Sayers, C. M., 2010, The effect of anisotropy on the Young’s moduli and Poisson’s ratios of shales: SEG.

- Sayers, C. M., K. Fisher, and J. J. Walsh, 2015, Rock physics of the Eagle Ford Shale: 85th Annual International Meeting, SEG, Expanded Abstracts, <https://doi.org/10.1190/segam2015-5827939.1>.
- Shoemaker, M., J. Peacock, and N. Zakhour, 2015, Integrating 3D seismic and geomechanical properties with microseismic acquisition and fracturing parameters to optimize completion practices within the Wolfcamp Shale Play of the Midland Basin: Presented at URTEC, <https://doi.org/10.15530/urtec-2015-2154184>.
- Singleton, S., 2018a, Geophysical data processing, rock property inversion, and geomechanical model building in a Midland Basin development project, Midland/Ector counties, Texas: *The Leading Edge*, **37**, no. 3, 182–189, <https://doi.org/10.1190/tle37030182.1>.
- Singleton, S., 2018b, Integration of geophysics and engineering for geomechanical earth modeling in a Midland Basin development project, Midland/Ector counties, Texas: Presented at URTEC, <https://doi.org/10.1190/tle37030182.1>.
- Thiercelin, M. J., and R. A. Plumb, 1994, A core-based prediction of lithologic stress contrasts in East Texas formations: *SPE*, **9**, no. 4, <https://doi.org/10.2118/21847-PA>.
- Thomsen, L., 2013, On the use of isotropic parameters λ , E , ν , and K to understand anisotropic shale behavior: 83rd Annual International Meeting, SEG, Expanded Abstracts, <https://doi.org/10.1190/segam2013-1080.1>.
- Vernik, L., 2016, Seismic petrophysics in quantitative interpretation: SEG, <https://doi.org/10.1190/1.9781560803256>.
- Warpinski, N. R., and L. W. Teufel, 1987, Influence of geologic discontinuities on hydraulic fracture propagation: *Journal of Petroleum Technology*, **39**, no. 2, <https://doi.org/10.2118/13224-PA>.
- Zoeppritz, K., 1919, Erdbebenwellen VII, VII B, Über reflexion und Durchgang seismischer Wellen durch Unstetigkeitsflächen: *Nachrichten der Königlichen Gesellschaft Wissenschaften zu Göttingen, Mathematischphysikalische Klasse*, 66–84.